Resource

Cell Reports

Engineering an Environment for the Study of Fibrosis: A 3D Human Muscle Model with Endothelium Specificity and Endomysium

Graphical Abstract

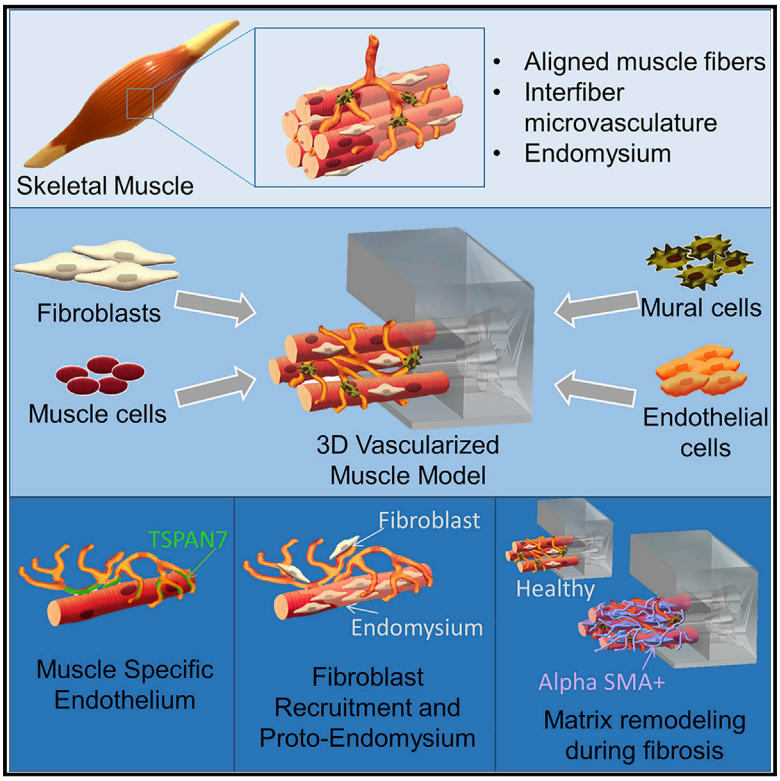

Highlights

- Millimeter-scale model of a vascularized 3D human muscle environment
- Endothelial cells acquire organ-specific signature in co-culture with muscle cells
- Muscle fibroblasts spontaneously self-assemble an endomysium-like structure
- Physiologically relevant 3D model for the study of muscle fibrosis

Authors

Simone Bersini, Mara Gilardi, Giovanni S. Ugolini, ..., Marco Vanoni, Giovanni Lombardi, Matteo Moretti

Correspondence

matteo.moretti@grupposandonato.it

In Brief

Bersini et al. demonstrate the generation of a mesoscale model of the human muscle environment and prove its application for the study of fibrosis. This engineered muscle environment promotes the organ-specific differentiation of endothelial cells and the self-assembly of myofibers spontaneously wrapped by a continuous endomysium-like structure.

Bersini et al., 2018, Cell Reports *25*, 3858–3868
December 26, 2018
https://doi.org/10.1016/j.celrep.2018.11.092

CellPress

OPEN ACCESS
CellPress

Cell Reports
Resource

Engineering an Environment for the Study of Fibrosis: A 3D Human Muscle Model with Endothelium Specificity and Endomysium

Simone Bersini,[1,10] Mara Gilardi,[1,2,10] Giovanni S. Ugolini,[3,10] Veronica Sansoni,[4] Giuseppe Talò,[1] Silvia Perego,[4] Simona Zanotti,[5] Paola Ostano,[6] Marina Mora,[5] Monica Soncini,[3] Marco Vanoni,[2,7] Giovanni Lombardi,[4] and Matteo Moretti[1,8,9,11,*]

[1]IRCCS Istituto Ortopedico Galeazzi, Cell and Tissue Engineering Laboratory, Milano, Italy
[2]PhD School in Life Sciences, University of Milano Bicocca, Milano, Italy
[3]Department of Electronics, Information and Bioengineering, Politecnico di Milano, Milano, Italy
[4]IRCCS Istituto Ortopedico Galeazzi, Laboratory of Experimental Biochemistry and Molecular Biology, Milano, Italy
[5]Muscle Cell Biology Laboratory, Neuromuscular Diseases and Neuroimmunology Unit, Fondazione IRCCS Istituto Neurologico C. Besta, Milano, Italy
[6]Cancer Genomics Laboratory, Fondazione Edo ed Elvo Tempia Valenta, Biella, Italy
[7]SYSBIO Centre for Systems Biology, Department of Biotechnology and Biosciences, University of Milano Bicocca, Milano, Italy
[8]Regenerative Medicine Technologies Lab, Ente Ospedaliero Cantonale, Lugano, Switzerland
[9]Swiss Institute for Regenerative Medicine, Lugano, Switzerland
[10]These authors contributed equally
[11]Lead Contact
*Correspondence: matteo.moretti@grupposandonato.it
https://doi.org/10.1016/j.celrep.2018.11.092

SUMMARY

The integration of vascular structures into *in vitro* cultured tissues provides realistic models of complex tissue-vascular interactions. Despite the incidence and impact of muscle-wasting disorders, advanced *in vitro* systems are still far from recapitulating the environmental complexity of skeletal muscle. Our model comprises differentiated human muscle fibers enveloped by a sheath of human muscle-derived fibroblasts and supported by a vascular network with mural-like cells. Here, we demonstrate the induction of muscle-specific endothelium and the self-organization of endomysial muscle fibroblasts mediated by endothelial cells. We use this model to mimic the fibrotic environment characterizing muscular dystrophies and to highlight key signatures of fibrosis that are neglected or underestimated in traditional 2D monocultures. Overall, this vascularized meso-scale cellular construct finely recapitulates the human skeletal muscle environment and provides an advanced solution for *in vitro* studies of muscle physiology and pathology.

INTRODUCTION

With muscle-wasting disorders currently representing a significant healthcare burden (Beaudart et al., 2014; Ryder et al., 2017), the search for effective reparative strategies still requires faithful *in vitro* models that include key physiological and pathological features. In this scenario, the integration of vascular structures and mesenchymal compartments into *in vitro* cultured tissues is of paramount importance, not only to ultimately engineer effective tissue constructs capable of integrating within a host body but also provide realistic models of complex interactions taking place in tissues of interest (e.g., angiogenesis or vasculogenesis in physiological or pathological tissues, tissue remodeling, and fibrosis) (Bersini et al., 2016b). As suggested by a recent investigation in mice, the endothelium displays organ-specific phenotype and architecture (Nolan et al., 2013) and takes part in the generation of vascular niches that secrete angiocrine factors involved in organ regeneration, homeostasis, and metabolism (Rafii et al., 2016). This often underestimated vessel-type and organ-specific differentiation of endothelial cells (ECs) has critical implications for understanding tissue development and homeostasis, as well as the onset of pathological conditions (Augustin and Koh, 2017; Potente and Mäkinen, 2017).

It is widely accepted that vascularized tissue models have more similarity with *in vivo* conditions and that tissue growth and maturation are deeply influenced by the presence of vasculature (Novosel et al., 2011). In skeletal muscles, vascular networks of ECs intertwine with bundled multinucleated muscle fibers (tens of microns in diameter) to ensure blood supply throughout muscle fascicles. Mesenchymal compartments also play crucial roles in tissue disease and homeostasis. In skeletal muscles, the mesenchymal compartment is constituted by muscle-supporting cells (fibroblasts and satellite cells) enclosed in a connective tissue sheath that covers muscle fibers (endomysium). This structure plays an important role in myogenesis and the regulation of tissue repair (Mathew et al., 2011; Murphy et al., 2011), and the cell types included represent major targets in regenerative therapies for muscle-wasting disorders (Yin et al., 2013) or pathological tissue remodeling (Mann et al., 2011). For instance, muscle diseases such as dystrophies crucially involve muscle fibroblasts and satellite cells that undergo progressive cycles of degeneration-regeneration, unbalance the production

of matrix proteins, and lead to abnormal replacement of muscle fibers with connective tissue containing collagen type I and fibronectin (Klingler et al., 2012; Zanotti et al., 2016). In this context, Duchenne muscular dystrophy (DMD) is a serious muscle-wasting disease caused by a mutation of the dystrophin gene on the X chromosome. The incidence of DMD is approximately 1 in 3,500 male newborns (Carnio et al., 2011). Although treatments aimed at improving patients' quality of life have been developed, there is still no effective cure and the median survival is <30 years (Rall and Grimm, 2012). Several works recently highlighted the importance of studying the cross-talk among multiple components of dystrophic muscles, emphasizing how targeting different cell types, including fibroblasts and ECs, would be fundamental to effectively address DMD (Shimizu-Motohashi and Asakura, 2014). In this framework, there is an increasing need for accurate *in vitro* models tailored to muscle pathologies. Research on dystrophies is widely based on animal models such as the mdx mouse, without a reliable human *in vitro* counterpart, except for simplistic bidimensional cultures of cells.

Attempts at biofabricating skeletal muscle tissues by co-culturing muscle cells and ECs have been reported (Visone et al., 2016). Tissue patches generated by co-culturing mouse myoblasts and ECs within an unarranged 3D matrix were shown to exhibit vessel-like structures (Levenberg et al., 2005; Shandalov et al., 2014; Perry et al., 2017). Endothelial cords surrounded by muscle bundles were obtained through microgrooved collagen scaffolds (Chen et al., 2017). Unorganized lumen structures were identified in 3D co-cultures of muscle cells and ECs (Carosio et al., 2013; Gholobova et al., 2015, 2018). Similar results were recently achieved by embedding, in a fibrin hydrogel under tension isogenic ECs, pericytes and myogenic cells obtained from human induced pluripotent stem cells (Maffioletti et al., 2018). Furthermore, perfusable microvascular networks of human ECs co-cultured with mouse myoblasts were developed within 3D hydrogels (Jeon et al., 2014, 2015). These models were not able to replicate the overall complexity of skeletal muscle. In fact, these approaches lack similarity with the human physiological tissue architecture, where the muscle compartment is organized into long fascicle-like structures intertwined with a vascular network and an extracellular matrix (ECM)-depositing mesenchymal tissue. Moreover, no *in vitro* model succeeded in demonstrating the organ specificity of the endothelium, a feature until now only described by an *in vivo* study in mice (Nolan et al., 2013). For these reasons, there is an urgent requirement for reliable models recreating a true skeletal muscle environment that combines proper muscle tissue organization, matrix-depositing mesenchymal cells, and organ-specific endothelial signatures in a human 3D context. The development of such a complex environment is necessary to analyze the heterogeneous interactions occurring among multiple cell types, which contribute to skeletal muscle tissue homeostasis and disorders.

Here, we describe the achievement of mesoscale skeletal muscle 3D constructs embedding differentiated muscle fibers and vascular networks exhibiting endothelial phenotypic specificity to muscle tissue. We demonstrate how this multicellular environment interacts with cells of mesenchymal origin. In particular, vascular networks mediate the recruitment of fibroblasts specifically derived from human muscles toward muscle fibers. Finally, we analyze matrix deposition by muscle fibroblasts derived from patients with DMD, highlighting through our model differences that were not detectable in traditional 2D assays.

RESULTS

Formation of Vascular Networks and Mature Muscle Fibers

Mesoscale systems were previously used for developing vascularized matrices (Underwood et al., 2014), including bone-mimicking tissue constructs (Bersini et al., 2016a; Bongio et al., 2016; Arrigoni et al., 2016). Our mesoscale system enables the casting of three non-planar fibers (600 μm diameter) of differentiated human muscle cells next to one another (600 μm distance between fibers) and the subsequent addition of hydrogels with embedded human ECs and supporting mesenchymal cells surrounding the fibers (Figures 1A–1C). More in detail, three muscle fibers were seeded by injecting human myoblasts embedded in human fibrin gel inside three cylindrical cavities formed in a sacrificial gel (Figure 1C). After sacrificial gel removal, suspended muscle fibers were differentiated for 5 days, allowing myoblast fusion into myotubes. For the vascular compartment, ECs were embedded in a fibrin-based hydrogel and pipetted inside the arch-shaped 3D structure surrounding the three muscle fibers after 5 days of differentiation. ECs were allowed to mature and organize in a microvascular network for an additional 3 or 6 days. Mesenchymal cells supporting the network partially differentiated into mural-like cells (Figure S1). Computational simulations of oxygen consumption-diffusion in the construct suggested that the oxygen level within the arch-shaped structure was above the critical threshold for cell survival (Carreau et al., 2011) (Figure 1B).

Muscle fibers underwent compaction from 600 μm diameter (hole dimension) to 137 ± 7 μm diameter after 5 days (Figure 2A). To demonstrate the compatibility with long-term culture, we analyzed muscle fibers up to day 34, highlighting an additional step of compaction compared to day 5 (68 ± 3 μm versus 137 ± 7 μm diameter). Viability for long-term culture was proved by LIVE (green)/DEAD (red) imaging after 34 days of culture (Figure 2B). As shown by histological sections, the bundle architecture (Figure 2C) more closely resembles the structure of the native muscle (Figure 2D) compared to muscle cells homogeneously embedded in a fibrin matrix (Figure 2E). Muscle fiber differentiation was demonstrated by the presence of terminally differentiated myotubes that were uniformly positive for myosin heavy chain (MHC) (Figures 2F and 2G), dystrophin, and alpha actinin (Figure S2). The calculated fusion index was equal to 50% ± 8%. Finally, we performed enzymatic digestion of tissue constructs, cell sorting, and cell-type-specific gene expression analysis to evaluate the phenotypic features of muscle fibers. More in detail, we carried out qRT-PCR analyses of genes relevant for basic muscular phenotype (desmin and myogenin factor 5 [MYF5]) (Figure 2H). The expression of these genes in the muscle cell population was compared to cultures of differentiated muscle cells alone (2D monocultures) or 2D co-cultures of ECs and differentiated muscle cells. The presence of ECs significantly increased the expression of desmin in muscle cells from 2D co-cultures compared to muscle cell monocultures

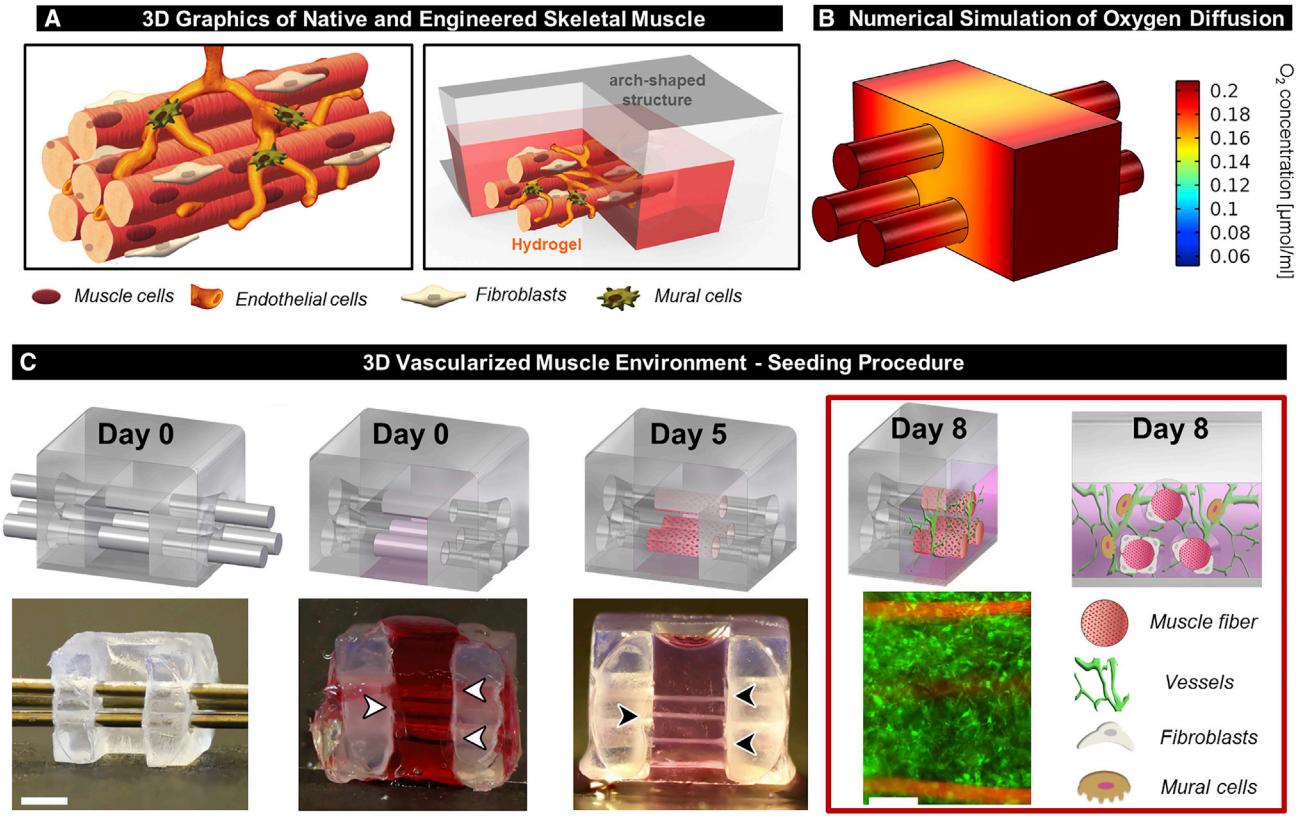

Figure 1. Design and Biofabrication of 3D Vascularized Muscle Model

(A) 3D graphics of skeletal muscle cellular architecture (left) with muscle cells arranged in packed muscle fibers intertwined with endothelial cells (ECs) forming blood capillaries. Mural cells support vascular structures, whereas fibroblasts are located in a connective sheath around muscle fibers. (Right) Target configuration of our human 3D vascularized muscle model. Three human differentiated muscle fibers are formed in a 3D hydrogel matrix (red) encased in a 3D printed arch-shaped mask (white) and surrounded by human endothelial microvascular networks. These networks are supported by human bone marrow-derived mesenchymal stem cells (MSCs) differentiated into mural cells and by human muscle-derived fibroblasts.

(B) Numerical simulation of oxygen consumption-diffusion within the 3D vascularized muscle model. Values of oxygen concentration within both hydrogel and muscle fibers are maintained above the critical threshold (0.052 μmol/mL) for cell survival.

(C) 3D vascularized muscle model seeding procedure: three steel rods are inserted in the arch-shaped structure side holes (scale bar, 2 mm) and used to cast three cylindrical cavities in gelatin sacrificial gel (day 0; gelatin colored with red dye for imaging purposes; white arrowheads indicate cylindrical cavities). High-density human muscle cells are injected in the cavities, gelatin is dissolved, and suspended muscle fibers (black arrowheads) are allowed to differentiate for 5 days (the cell culture medium appears pink in the image). Finally, human EC-laden fibrin gel is pipetted into the central structure gap to surround the three fibers. After 3 days of maturation vascular networks are formed and surround muscle fibers (day 8; scale bar, 500 μm).

Representative images obtained from >200 independent samples. See also Figure S1.

($p < 0.001$). The expression of desmin was even higher in muscle cells from 3D co-cultures compared to 2D co-cultures ($p = 0.01$), indicating an additive effect due to the dimensionality of the system. However, the expression of MYF5 was not affected either by the presence of ECs or the dimensionality of the system. Overall, these results show that the co-culture of muscle cells with ECs positively influences muscle differentiation (analysis performed at day 8).

After the addition and maturation of ECs, the resulting 3D constructs were characterized by means of confocal imaging. ECs developed a network (Figures 3A and 3B) of microvessels (Figure 3C), which wrapped and connected to muscle fibers (Figure 3D; Video S1), hence recapitulating the *in vivo* architecture of the muscle tissue, where capillary structures intertwine among single muscle fibers. Overall, the model presented here clearly shows that vessels rapidly organize into interconnected microvascular networks with lumen-like structures (Figure 3C), which not only passively surround muscle fibers but also connect to and align on their surface (Figure 3D). Co-culturing ECs with non-bundled, randomly distributed muscle cells in a fibrin hydrogel only led to the formation of sparse and disconnected branches of microvessels (Figure S3).

To evaluate the role of mesenchymal cells in interacting with the microvascular network, ECs were mixed with either human bone marrow-derived mesenchymal stem cells (MSCs) or muscle-derived human fibroblasts. Parameters of vascular networks (total network length, diameter, and area covered) found near muscle fibers (600 × 600 μm^2 regions centered on muscle fibers) and quantified from confocal images (Figures 3E and S4) demonstrated that MSCs modified network properties mainly by

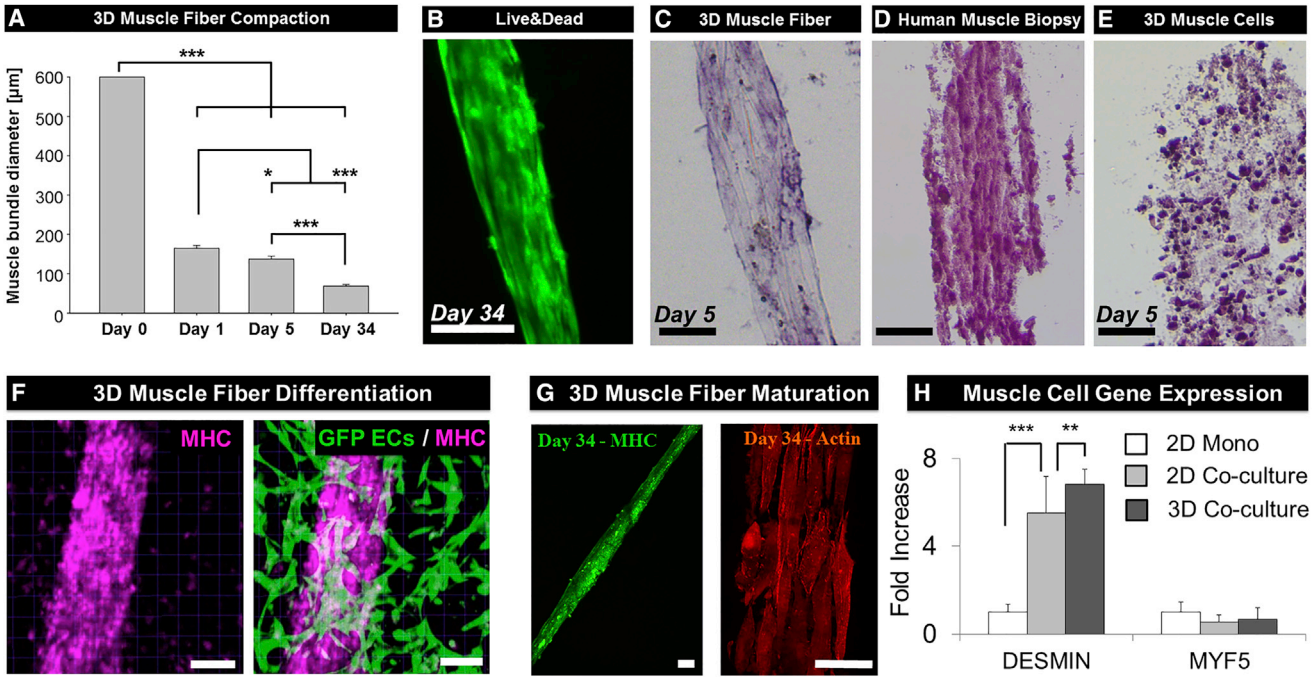

Figure 2. Characterization of the Muscle Compartment

(A) Compaction of muscle fibers with time. From a starting diameter of 600 μm, human muscle cells progressively compact the matrix and exhibit diameters of approximately 140 μm (day 5) and 70 μm (day 34). Data collected from at least three independent experiments. ANOVA test performed to quantify statistical differences.

(B) LIVE/DEAD staining of muscle fibers demonstrating cell viability for long-term culture (day 34). Viable cells appear in green. No dead cells (red signal) are detected. Scale bars, 100 μm.

(C–E) Histological sections of different 3D organizations of muscle cells. 3D *in vitro* muscle fibers (C) show aligned and elongated myotubes more closely resembling the *in vivo* architecture (D) compared to muscle cells homogeneously embedded and differentiated in a 3D fibrin hydrogel (E).

(F) Muscle fiber differentiation evaluated by immunostaining for myosin heavy chain (MHC, pink). Muscle fibers exhibit myotubes uniformly positive for MHC. Green, ECs.

(G) Long-term cultured muscle fibers (red, actin) showing positive MHC immunostaining (green), an indication of muscle differentiation.

(H) Gene expression analyses performed on muscle cells (desmin and MYF5). Fold increase relative to housekeeping gene RPL32 versus 2D muscle cell culture only.

Gene expression data were obtained from three independent experiments. Unpaired t test was performed to quantify statistical differences. Scale bars, 100 μm (except 50 μm for G). Error bars represent SEMs. *$p < 0.05$, **$p < 0.01$, ***$p < 0.001$.

See also Figure S2.

narrowing vessel diameters. The length/diameter ratio was significantly higher in the presence of MSCs with respect to ECs networks without MSCs (330.2 ± 30.2 versus 228.3 ± 3.9; $p < 0.001$ [day 11]) (Figure 3E). However, muscle-derived fibroblasts succeeded in populating the constructs while maintaining stable vascular network parameters. No statistical differences were found in length/diameter ratio values in constructs seeded with ECs only and ECs mixed with muscle-derived fibroblasts (day 11). In addition, the area covered by vascular networks in the presence of muscle-derived fibroblasts increased from day 8 to day 11. The area covered was lower compared to vascular networks with MSCs (day 11), although without a statistical difference (Figure 3E).

Vascular Networks Acquire Organ-Specific Phenotypic Signature

A recent study has shown that *in vivo* endothelia are characterized by organ-specific genotypic and phenotypic signatures that drive important organotypic features of the vascular compartment (e.g., expression of specific genes and proteins, fenestrations, junctions, network sizes) (Nolan et al., 2013). To date, none of the approaches aimed at forming vascularized models successfully reproduced organ-specific ECs *in vitro*. To evaluate phenotypic features of ECs, we performed enzymatic digestion of tissue constructs, cell sorting, and cell-type-specific gene expression analysis. As a first step, we performed qRT-PCR analyses of genes relevant for endothelial phenotypes (CD36, CD31) (Figure 4A). These genes were consistently expressed by ECs cultured in the 3D vascularized muscle model, with levels of expression comparable to 3D EC monocultures (CD36) and even higher (CD31, $p < 0.05$) (Figure 4A), demonstrating that the presence of muscle cells did not negatively influence the expression of endothelial-specific genes. Primary human ECs from muscle biopsies were used as an additional control, showing similar values of CD31 gene expression when compared with 3D EC monocultures. The expression level of

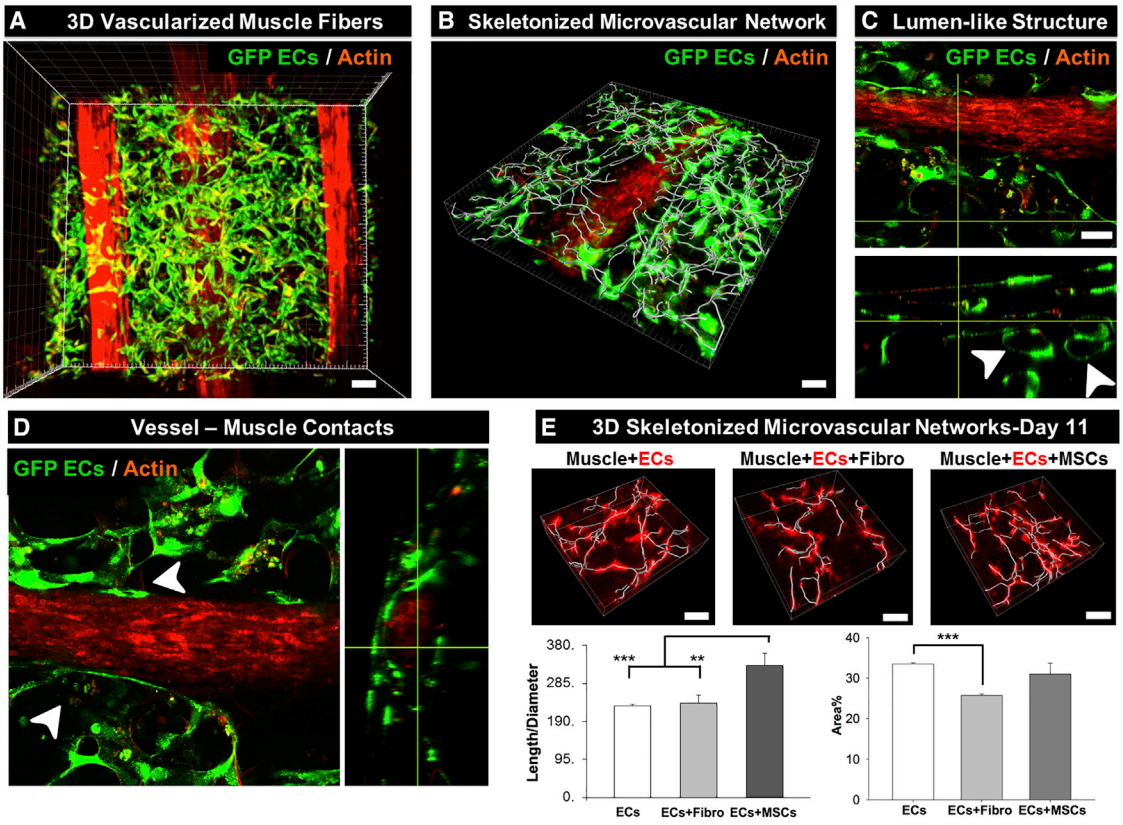

Figure 3. Confocal Imaging and Characterization of the 3D Vascularized Muscle Model

(A) Confocal reconstruction of the whole system embedding muscle cells (red, actin staining) and ECs (green). ECs self-organize in a uniform vascular network enclosing the three muscle fibers.

(B) 3D skeletonization of the microvascular network surrounding a muscle fiber. Muscle cells (red, actin staining) and ECs (green).

(C) Microvessels show lumen-like structures. Top view of representative microvessels and confocal reconstruction of the cross-section showing how ECs form hollow vessels with lumens (white arrowheads). Muscle cells (red, actin staining) and ECs (green).

(D) Detailed imaging of the contact between ECs and muscle cells in the vascularized muscle construct. Muscle fibers (red, actin) wrapped by microvessels (green, ECs) showing ECs-muscle contacts (white arrowheads) from top view (left) and reconstructed cross-section (right).

(E) Histogram graphs of network parameters (area coverage and length/diameter ratio) quantified from images of vascular networks at day 11 under different co-culture conditions with muscle cells (ECs, ECs + muscle-derived fibroblasts, ECs + mesenchymal stem cells [MSCs]). ANOVA test was performed to compare conditions.

Network parameters extracted from at least three independent experiments. Scale bars, 100 μm. Error bars represent SEMs. $^{**}p < 0.01$, $^{***}p < 0.001$.

See also Figures S3 and S4.

CD36 resulted higher in primary muscle ECs compared to *in vitro* cultured ECs (Figure 4A).

In addition, we quantified the expression of genes peculiar to *in vivo* muscle-specific ECs (tetraspanin 7 [TSPAN7] and peroxisome proliferator-activated receptor gamma [PPARG]) (Figure 4A). Primary ECs extracted from human muscle biopsies exhibited high levels of TSPAN7 (genetic footprint of muscle-derived ECs) compared to 3D EC monocultures, as expected. The expression level of TSPAN7 was also significantly upregulated in the 3D vascularized muscle model compared to 3D EC monocultures ($p < 0.05$; Figure 4A). PPARG was also upregulated in ECs collected from the 3D vascularized muscle model compared to 3D EC monocultures ($p = 0.09$; Figure 4A), recapitulating differences observed in mice by Nolan et al. (2013). However, it should be considered that our analyses of human primary ECs from muscle biopsies showed lower values of PPARG compared to ECs from the 3D vascularized muscle model. Additional microarray analyses were performed to compare the gene expression of primary ECs extracted from muscle biopsies and ECs from the 3D vascularized muscle model. We found that key genes characterizing the muscle specificity of ECs (Nolan et al., 2013) were not differentially expressed in the two groups ($\log_2FC > 1$ or $\log_2FC < -1$, adjusted p value < 0.01; Table S1). These genes include TSPAN7 and also fetal liver kinase-1 (FLK1), laminin subunit alpha-4 (LAMA4), fibroblast growth factor-9 (FGF9), activating transcription factor-3 (ATF3), T-box transcription factor-3 (TBX3), phosphatidate cytidylyltransferase 1 (CDS1), ETS domain-containing protein Elk-3 (ELK3), and C-X-C chemokine receptor type 7 (CXCR7). These data show that data co-culture with muscle cells is able to initiate a differentiation program leading to muscle-specific endothelia. Based on this microarray analysis, we selected four genes that are

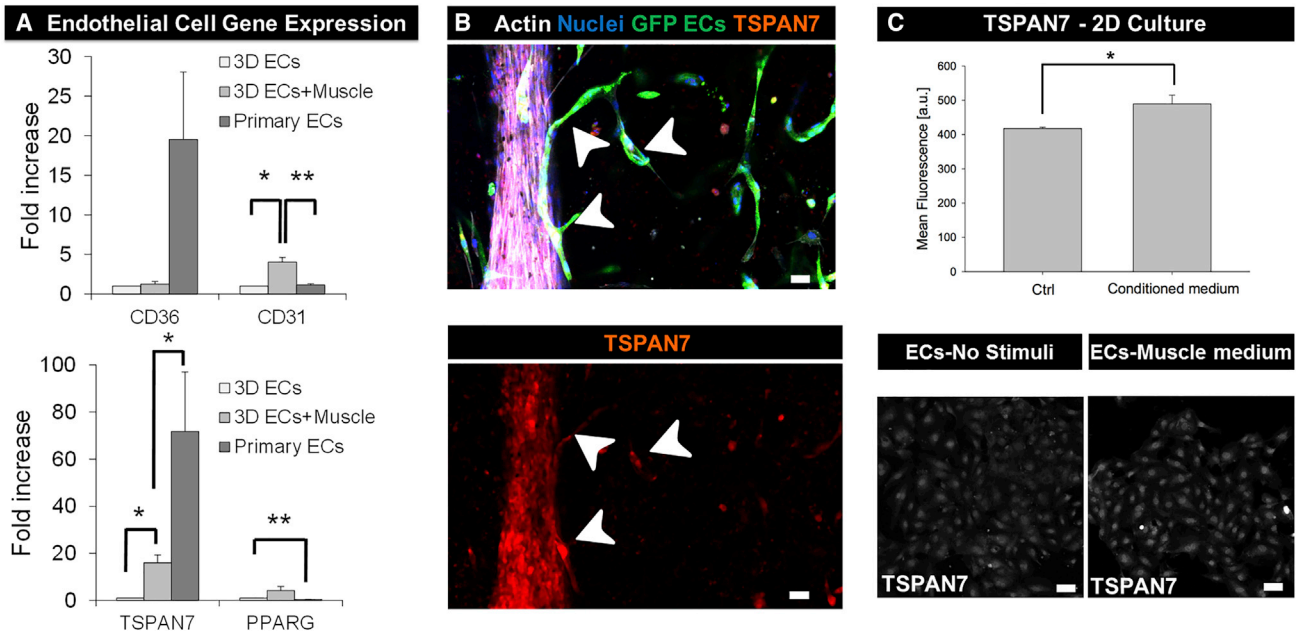

Figure 4. Characterization of the Vascular Compartment

(A) Gene expression qRT-PCR analyses performed on ECs (CD36, CD31, TSPAN7, and PPARG) isolated from ECs monocultured in 3D, from the 3D vascularized muscle model, and from ECs derived from human muscle biopsies. Fold increase relative to housekeeping gene RPL32 versus 3D EC monoculture. Gene expression data were obtained from three independent experiments. ANOVA test was performed to quantify statistical differences.

(B) 3D vascularized muscle model showing the presence of TSPAN7$^+$ ECs (red) in contact with the muscle fiber. Green, ECs; white, actin; blue, nuclei.

(C) TSPAN7 expression quantified through immunofluorescence within monolayers of ECs incubated with muscle cell conditioned medium or control medium (no stimuli). Scale bars, 50 μm.

Data obtained from four independent samples. Unpaired t test was performed to compare conditions. Error bars represent SEMs. *$p < 0.05$, **$p < 0.01$.

See also Figures S5 and S6.

typical of EC muscle-specific differentiation and compared their expression at the protein level in undifferentiated EC monocultures versus ECs co-cultured with muscle cells. Our data clearly show a significant increase in these target proteins in the EC population upon co-culture with muscle cells (Figure S5).

Finally, we found TSPAN7$^+$ ECs in immunofluorescent images of the 3D vascularized muscle model. In particular, we identified the brightest cells in close proximity to muscle fibers (Figure 4B). We hypothesize that the muscle-induced expression of TSPAN7 is at least in part related to cell-cell paracrine interactions and gradients of muscle-secreted molecules. We found that EC monolayers treated with muscle cell conditioned media were characterized by higher TSPAN7 expression compared to ECs treated with control medium ("no stimuli") (490 ± 11 versus 410 ± 2) (Figure 4C).

ECs Mediate the Recruitment of Muscle-Specific Fibroblasts

To investigate potential effects due to the presence of ECs in our 3D construct, we mixed muscle-derived human fibroblasts with ECs. Homogeneously distributed muscle-derived human fibroblasts progressively migrated toward muscle fibers (day 8) and finally adhered to the outer part of the fibers generating a sheath (day 11) (Figure 5A), which resembled the *in vivo* localization of the connective endomysium (Agley et al., 2013). Of note, this fibroblasts-muscle fiber interaction was not observed in constructs embedding lung-derived fibroblasts in the presence of ECs (Figure 5B) or in constructs embedding muscle-derived fibroblasts without ECs (Figure 5C). The area covered by muscle fibroblasts in vascularized constructs was significantly higher compared to the area covered by lung fibroblasts in vascularized tissue constructs (95.1% ± 2.3% versus 8.98% ± 3.15%) or by muscle fibroblasts in avascular tissue constructs (95.1% ± 2.3% versus 16.12% ± 4.72%) (Figure 5D). Overall, these data demonstrate that ECs are critical for recreating specific cellular interactions and physiological cross-talk in tissue-like models.

DMD-Derived Muscle Fibroblasts Show Increased Matrix Deposition in Vascularized Muscle Constructs Compared to Standard Culture

Muscular dystrophies including DMD are characterized by an unbalanced production of matrix proteins that leads to the abnormal replacement of muscle fibers with connective tissue. At present, no *in vitro* model is able to reliably analyze the deposition of ECM proteins, with the exception of simplistic bidimensional cultures.

For this reason, we challenged the 3D vascularized muscle model with pathological conditions by embedding in the 3D constructs muscle fibroblasts derived from a single DMD patient, rather than from a healthy subject (no changes were introduced for the other components of the model). Fibroblasts are mainly responsible for the deposition of ECM components. Hence, we

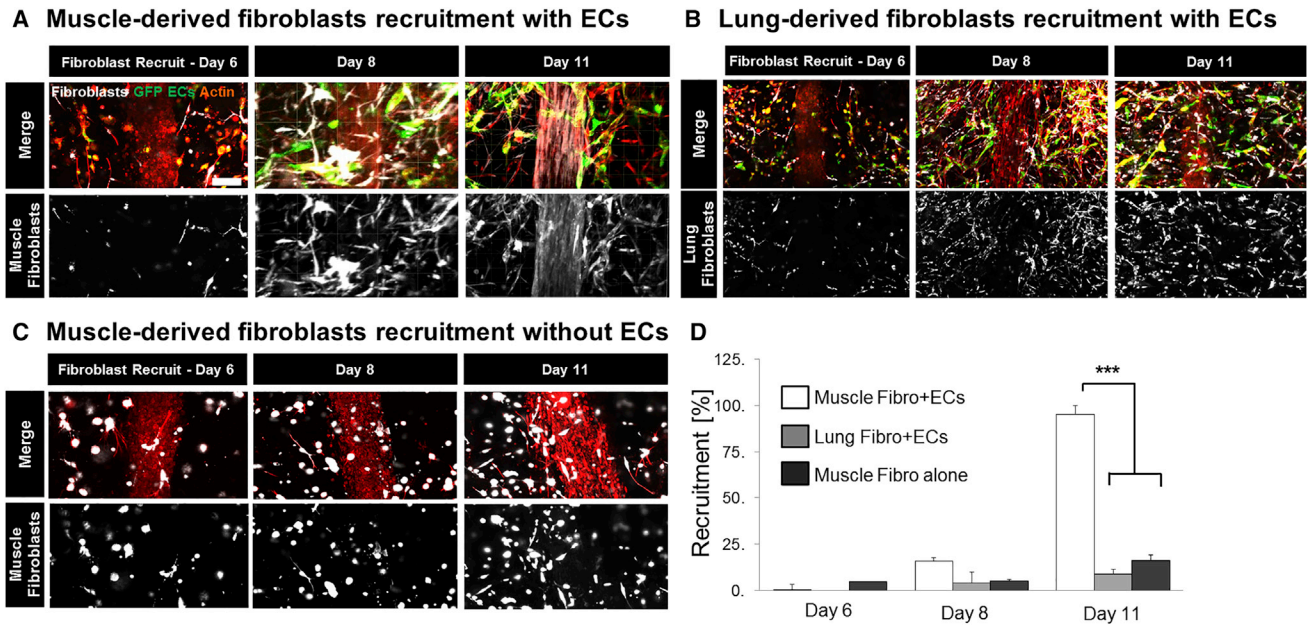

Figure 5. Fibroblast Recruitment to Muscle Fibers

(A) Distribution of human muscle-derived fibroblasts in the 3D vascularized muscle model at days 8 and 11. Vybrant cell labeling was used to specifically track human muscle-derived fibroblasts (white). Actin staining (red) highlights all of the cell populations, including differentiated muscle fibers, while ECs are shown in green.

(B) Human lung-derived fibroblasts recruitment in the 3D vascularized muscle model.

(C) Distribution of human muscle-derived fibroblasts in the 3D muscle model without ECs.

(D) Quantification of fibroblast recruitment in the conditions shown in (A), (B), and (C).

Scale bar, 100 μm. Data obtained from at least three independent experiments. ANOVA test was performed to quantify statistical differences. Error bars represent SEMs. ***$p < 0.001$.

hypothesized that introducing pathological fibroblasts without changes in other components of the systems would have allowed the reproduction of key features of fibrosis observed *in vivo*. In parallel, we stimulated healthy 3D vascularized muscle constructs with 10 ng/mL transforming growth factor beta 1 (TGF-β1), a known inducer of fibrotic responses in fibroblasts of different origin and generally used as the gold standard for mimicking tissue fibrosis in cell cultures (Zanotti et al., 2016). The main goal of the following analysis was to study how different cell types (e.g., healthy fibroblasts, TGF-β1-treated fibroblasts, DMD fibroblasts) deposit ECM proteins and demonstrate that the 3D vascularized muscle model could be effectively used to investigate fibrosis. Collagens and fibronectin represent major components of fibrotic matrices. In addition, dystrophic muscles are characterized by the presence of myofibroblasts whose main marker is α-smooth muscle actin (Wynn, 2008). For this reason, we decided to analyze and compare the presence of these markers in each experimental condition.

The expression of collagen I in vascularized muscle tissues containing DMD fibroblasts was significantly higher compared to both control ($p < 0.001$) and TGF-β1-treated samples ($p < 0.001$) (Figures 6A and 6B). In a similar way, tissue constructs with embedded DMD fibroblasts highlighted a significantly higher level of fibronectin compared to control ($p < 0.001$) and TGF-β1-treated ($p < 0.001$) samples (Figures 6A and 6B). Moreover, DMD fibroblasts showed higher expression of α-smooth muscle actin compared to control fibroblasts ($p < 0.001$), which is an indication of differentiation toward a pathological myofibroblast condition (Figures 6A and 6B). These results demonstrate that the 3D vascularized muscle model with embedded pathological fibroblasts is able to recapitulate the upregulation of key markers of fibrosis. The DMD fibroblasts secreted even more collagen I and fibronectin compared to tissue constructs treated with TGF-β1, which is considered the optimal treatment to induce tissue fibrosis *in vitro*.

The same analyses were performed in 2D models, based on the co-culture of ECs and fibroblasts on top of monolayers of differentiated muscle cells. Fibroblast monocultures or co-cultures of muscle cells and fibroblasts (without ECs) represent the gold standard in current muscle fibrosis experiments. No clear differences were observed in terms of matrix deposition between DMD and control fibroblasts. Collagen I expression only showed a positive trend in DMD fibroblasts compared to control cells (Figures 6C and 6D). A similar trend was quantified for α-smooth muscle actin, even though no statistical differences were detected (Figures 6C and 6D). Hence, these results did not replicate differences observed through the 3D vascularized muscle model. In addition, in contrast to 3D experiments, the α-smooth muscle actin content was significantly higher in TGF-β1-treated samples compared to DMD fibroblasts ($p < 0.05$). Finally, the amount of fibronectin in DMD and control samples was comparable (Figures 6C and 6D).

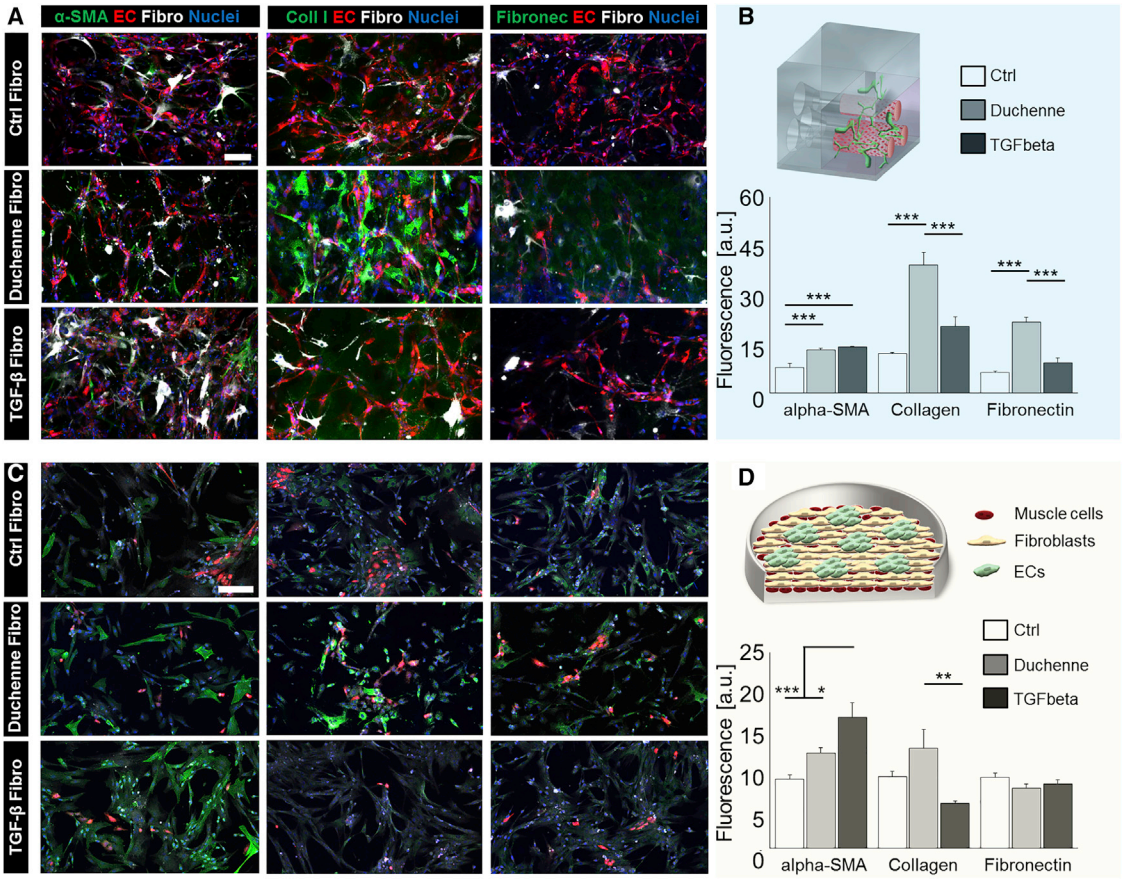

Figure 6. Application of the 3D Vascularized Muscle Model for the Study of Fibrosis

(A and B) Confocal imaging (A) and quantification (B) of fibrotic markers (green, α-smooth muscle actin, collagen I, and fibronectin) in the 3D model with embedded control (ctrl) fibroblasts, Duchenne fibroblasts, or TGF-β1-treated fibroblasts (white, Vybrant cell labeling to specifically track fibroblasts). Red, ECs; blue, nuclei.

(C and D) Confocal imaging (C) and analysis (D) of fibrotic markers in the 2D model.

Scale bars, 100 μm. Data obtained from at least three independent experiments. ANOVA test was performed to quantify statistical differences. Error bars represent SEMs. *p <0.05, **p < 0.01, ***p < 0.001.

Overall, we have demonstrated that tissue constructs with embedded DMD fibroblasts are able to secrete key ECM proteins such as collagen I and fibronectin. Furthermore, confocal imaging revealed that the amount of secreted proteins was higher with DMD fibroblasts compared to healthy fibroblasts. Finally, the comparison between our 3D vascularized muscle model and a simplified 2D co-culture showed that our approach is able to capture differences that are reduced or even neglected in traditional 2D models. However, we should also consider that the cells used here were derived from a single donor and that further analyses using cells from multiple patients will be required to confirm the differences between biological groups.

DISCUSSION

The development of complex and faithful pathophysiological models represents a key challenge to improve the outcome of basic and translational research. Musculoskeletal tissue has a distinctive 3D architecture that is characterized by muscle fibers surrounded by a fibroblast-rich endomysium and intertwined with microvascular networks. This spatial organization is fundamental to maintain the functionality of the muscle tissue and can be reproduced by advanced 3D models and tissue constructs. Here, we report a method for biofabricating *in vitro* 3D human vascularized skeletal muscle environments that exhibit not only a more *in vivo*-like architecture but also fundamental physiological features that were previously overlooked. Building on previous models based on single muscle fibers or sheets (Madden et al., 2015; Neal et al., 2014), we showed how to include a self-organizing vascular network that wraps multiple non-planar differentiated muscle fibers. As demonstrated by the trend of fiber compaction (Figure 2A) and by confocal imaging (Figures 2F, 2G, and S2), the engineered muscle tissue constructs are gradually differentiating toward *in vivo*-like muscle fibers.

We demonstrated how human ECs forming vascular networks within the *in vitro* muscle model are induced to acquire phenotypic characteristics of *in vivo* muscle ECs. This phenotypic modulation was previously observed only in *in vivo* experiments,

and no other *in vitro* report addressed the organ or muscle specificity of ECs. We have preliminarily investigated putative mechanisms responsible for this phenotypic change; co-culture of ECs with muscle cells induced upregulated expression of target genes (TSPAN7 and PPARG). We hypothesize the existence of a paracrine action exerted by muscle cells on ECs, as suggested by an increase in target proteins in ECs cultured with muscle-conditioned media. Microarray and western blot analyses confirmed that ECs co-cultured with muscle cells were actually differentiating toward a muscle-specific endothelial phenotype.

We explored the importance of including the vascular compartment by analyzing the response of cells of mesenchymal origin in our vascularized muscle construct. Human muscle-derived fibroblasts were embedded in the fibrin gel surrounding the fibers, together with ECs. This construct formulation allowed for the vascular network to form without major structural alterations, as analyzed by network parameters (Figures 3E and S4). We observed how muscle-derived fibroblasts migrated toward muscle fibers, forming an enveloping sheath that mimics the endomysium. Our 3D model allowed us to identify a key effect of the heterotypic cross-talk among ECs, muscle fibroblasts, and muscle cells. We were able to recapitulate the organotypic process driving muscle-specific fibroblast recruitment toward differentiated muscle fibers, while lung-specific fibroblasts were not able to migrate and wrap muscle cells. Fibroblast recruitment was observed only when vasculature was present in the system, thus demonstrating that introducing a vascular compartment does not merely represent the attempt to model a vascularized tissue but has critical consequences on the physiological behavior of specific cell types. These results also extend recent findings that vascular cells can increase myogenesis and muscle contraction of *in vitro*-cultured mouse muscle cells (Osaki et al., 2018).

The behavior of fibroblasts in skeletal muscles is known to play a key role in muscle-wasting disorders, particularly in the replacement of functional muscle cells with ECM-based, non-contractile connective tissue (Grounds, 2008; Zanotti et al., 2016). Conventional 2D assays are generally limited to the study of the intracellular levels of specific proteins (Stahnke et al., 2017), since the lack of 3D architectural arrangement does not allow the quantification of the 3D accumulation and the distribution of proteins in the surrounding environment (Bersini et al., 2018). In this framework, the lack of a physiological 3D matrix in which secreted proteins can gradually accumulate could reduce the differences between experimental groups. Herein, we have exploited our 3D model to show that the inclusion of DMD-derived fibroblasts (without changing any other cellular component of the system) is sufficient to significantly increase the expression level of fibrosis-associated proteins, such as collagen I and fibronectin, compared to control or TGF-β1-treated fibroblasts. We demonstrated that statistical differences in terms of collagen I, fibronectin, and α-smooth muscle actin between 3D constructs embedding DMD fibroblasts or control healthy muscle fibroblasts were not detected in 2D co-culture experiments. According to conventional 2D assays, TGF-β1 appears to be in principle a good strategy to mimic pathological DMD fibroblasts. Our results in terms of α-smooth muscle actin seem to confirm this assumption. However, the expression of collagen I in TGF-β1-treated samples was significantly different compared to samples with DMD fibroblasts, and no clear differences were detected in terms of fibronectin. In contrast, our 3D tissue constructs reveal that the expression of both collagen I and fibronectin in TGF-β1-treated fibroblasts was significantly lower compared to DMD fibroblasts ($p < 0.001$), while no changes were detected in terms of α-smooth muscle actin. In addition, clear differences were always detectable when comparing samples with healthy and DMD fibroblasts. Overall, we were able to show that DMD fibroblasts embedded in a 3D vascularized muscle environment recapitulate the abnormal fibrotic deposition of ECM proteins, including collagen I and fibronectin. In addition, DMD fibroblasts express α-smooth muscle actin, a key hallmark of differentiation toward a myofibroblast phenotype. Collected data thus show that traditional 2D assays may overlook or bias critical aspects of cell behavior that are instead captured in our 3D vascularized muscle environment.

Future work may be directed to overcome the present limitations of the model. For instance, this system was not specifically designed to create contractile muscle fibers or to control perfusion through patent vessels. As previously reported by others, the addition of biochemical (e.g., Matrigel) (Madden et al., 2015) and biophysical (e.g., electrical field) (Neal et al., 2014) stimuli is critical to promote muscle fiber contraction. However, the generation of contractile muscle fibers was not directly required to reproduce and analyze the heterotypic interactions among each component of the muscle environment.

In conclusion, we have highlighted evidence of endothelial organ specificity and muscle-specific fibroblast recruitment, which were not previously observed *in vitro*. These results were obtained through a model of vascularized muscle that presents high levels of similarity with the physiological muscle environment. The key features of the model—architecture of the system and multiple players involved—were overlooked by all previous reports and come together in a comprehensive 3D human vascularized skeletal muscle environment, which is relevant in exploring muscle fibroblast physiological and pathological behavior during fibrosis. The model presented here proved to be compatible not only with high-resolution imaging techniques and analyses of matrix deposition but also with cell-type-specific mRNA retrieval for in-depth gene expression analyses. It is thus expected to bring significant advances to basic skeletal muscle research as well as to the pipeline of drug discovery and/or screening for muscle disorders.

STAR★METHODS

Detailed methods are provided in the online version of this paper and include the following:

- KEY RESOURCES TABLE
- CONTACT FOR REAGENT AND RESOURCE SHARING
- EXPERIMENTAL MODEL AND SUBJECT DETAILS
  - Human subjects
  - Cell isolation and culture
- METHOD DETAILS
  - Construct frame fabrication
  - Computational simulations

SUPPLEMENTAL INFORMATION

Supplemental Information includes six figures, one table, and one video and can be found with this article online at https://doi.org/10.1016/j.celrep.2018.11.092.

ACKNOWLEDGMENTS

Funding from the Italian Ministry of Health is gratefully acknowledged. This work was supported by the Office of the Assistant Secretary of Defense for Health Affairs through the Breast Cancer Research Program under award no. W81XWH-15-1-0092. Opinions, interpretations, conclusions, and recommendations are those of the authors and are not necessarily endorsed by the Department of Defense. Human muscle cells were a kind gift of Prof. Gabellini (San Raffaele Hospital, Milano, Italy). The authors would like to thank Prof. Gabellini and Dr. Ferri for useful discussions and suggestions on muscle cell culture. EuroBioBank and the Telethon Network of Genetic Biobanks (GTB12001F) are gratefully acknowledged for providing DMD muscle-derived fibroblasts. Primary cells used in this study were collected upon approval of the Ethics Committee of the San Raffaele Hospital (April 2015). Two-photon confocal imaging was performed in the Advanced Light and Electron Microscopy BioImaging Center (ALEMBIC) at San Raffaele Hospital (Milano, Italy) with the help of Dr. Covino. Microarray analyses were performed with the help of Dr. Giovanna Chiorino (Cancer Genomics Lab at Fondazione Edo ed Elvo Tempia Valenta, Biella, Italy).

AUTHOR CONTRIBUTIONS

S.B., M.G., G.S.U., and M. M. designed the study. S.B., M.G., and G.S.U. performed the experiments and analyzed the data. V.S., G.T., S.P., S.Z., P.O., M.M., M.S., M.V., and G.L. collaborated on some experiments and data analysis. S.B., G.S.U., and M.M. wrote the manuscript.

DECLARATION OF INTERESTS

The authors declare no competing interests.

Received: February 27, 2018
Revised: October 16, 2018
Accepted: November 27, 2018
Published: December 26, 2018

REFERENCES

Abaci, H.E., Truitt, R., Tan, S., and Gerecht, S. (2011). Unforeseen decreases in dissolved oxygen levels affect tube formation kinetics in collagen gels. Am. J. Physiol. Cell Physiol. *301*, C431–C440.

Agley, C.C., Rowlerson, A.M., Velloso, C.P., Lazarus, N.R., and Harridge, S.D. (2013). Human skeletal muscle fibroblasts, but not myogenic cells, readily undergo adipogenic differentiation. J. Cell Sci. *126*, 5610–5625.

Arrigoni, C., Bongio, M., Talò, G., Bersini, S., Enomoto, J., Fukuda, J., and Moretti, M. (2016). Rational Design of Prevascularized Large 3D Tissue Constructs Using Computational Simulations and Biofabrication of Geometrically Controlled Microvessels. Adv. Healthc. Mater. *5*, 1617–1626.

Augustin, H.G., and Koh, G.Y. (2017). Organotypic vasculature: from descriptive heterogeneity to functional pathophysiology. Science *357*, eaal2379.

Beaudart, C., Rizzoli, R., Bruyère, O., Reginster, J.Y., and Biver, E. (2014). Sarcopenia: burden and challenges for public health. Arch. Public Health *72*, 45.

Bersini, S., Gilardi, M., Arrigoni, C., Talò, G., Zamai, M., Zagra, L., Caiolfa, V., and Moretti, M. (2016a). Human in vitro 3D co-culture model to engineer vascularized bone-mimicking tissues combining computational tools and statistical experimental approach. Biomaterials *76*, 157–172.

Bersini, S., Yazdi, I.K., Talò, G., Shin, S.R., Moretti, M., and Khademhosseini, A. (2016b). Cell-microenvironment interactions and architectures in microvascular systems. Biotechnol. Adv. *34*, 1113–1130.

Bersini, S., Gilardi, M., Mora, M., Krol, S., Arrigoni, C., Candrian, C., Zanotti, S., and Moretti, M. (2018). Tackling muscle fibrosis: from molecular mechanisms to next generation engineered models to predict drug delivery. Adv. Drug Deliv. Rev. *129*, 64–77.

Bongio, M., Lopa, S., Gilardi, M., Bersini, S., and Moretti, M. (2016). A 3D vascularized bone remodeling model combining osteoblasts and osteoclasts in a CaP nanoparticle-enriched matrix. Nanomedicine (Lond.) *11*, 1073–1091.

Carnio, S., Serena, E., Rossi, C.A., De Coppi, P., Elvassore, N., and Vitiello, L. (2011). Three-dimensional porous scaffold allows long-term wild-type cell delivery in dystrophic muscle. J. Tissue Eng. Regen. Med. *5*, 1–10.

Carosio, S., Barberi, L., Rizzuto, E., Nicoletti, C., Del Prete, Z., and Musarò, A. (2013). Generation of eX vivo-vascularized Muscle Engineered Tissue (X-MET). Sci. Rep. *3*, 1420.

Carreau, A., El Hafny-Rahbi, B., Matejuk, A., Grillon, C., and Kieda, C. (2011). Why is the partial oxygen pressure of human tissues a crucial parameter? Small molecules and hypoxia. J. Cell. Mol. Med. *15*, 1239–1253.

Chen, S., Kawazoe, N., and Chen, G. (2017). Biomimetic Assembly of Vascular Endothelial Cells and Muscle Cells in Microgrooved Collagen Porous Scaffolds. Tissue Eng. Part C Methods *23*, 367–376.

Colom, A., Galgoczy, R., Almendros, I., Xaubet, A., Farré, R., and Alcaraz, J. (2014). Oxygen diffusion and consumption in extracellular matrix gels: implications for designing three-dimensional cultures. J. Biomed. Mater. Res. A *102*, 2776–2784.

Ferri, G., Huichalaf, C.H., Caccia, R., and Gabellini, D. (2015). Direct interplay between two candidate genes in FSHD muscular dystrophy. Hum. Mol. Genet. *24*, 1256–1266.

Gholobova, D., Decroix, L., Van Muylder, V., Desender, L., Gerard, M., Carpentier, G., Vandenburgh, H., and Thorrez, L. (2015). Endothelial Network Formation Within Human Tissue-Engineered Skeletal Muscle. Tissue Eng. Part A *21*, 2548–2558.

Gholobova, D., Gerard, M., Decroix, L., Desender, L., Callewaert, N., Annaert, P., and Thorrez, L. (2018). Human tissue-engineered skeletal muscle: a novel 3D in vitro model for drug disposition and toxicity after intramuscular injection. Sci. Rep. *8*, 12206.

Grounds, M.D. (2008). Two-tiered hypotheses for Duchenne muscular dystrophy. Cell. Mol. Life Sci. *65*, 1621–1625.

Jeon, J.S., Bersini, S., Whisler, J.A., Chen, M.B., Dubini, G., Charest, J.L., Moretti, M., and Kamm, R.D. (2014). Generation of 3D functional microvascular networks with human mesenchymal stem cells in microfluidic systems. Integr. Biol. *6*, 555–563.

Jeon, J.S., Bersini, S., Gilardi, M., Dubini, G., Charest, J.L., Moretti, M., and Kamm, R.D. (2015). Human 3D vascularized organotypic microfluidic assays to study breast cancer cell extravasation. Proc. Natl. Acad. Sci. USA *112*, 214–219.

Klingler, W., Jurkat-Rott, K., Lehmann-Horn, F., and Schleip, R. (2012). The role of fibrosis in Duchenne muscular dystrophy. Acta Myol. *31*, 184–195.

Levenberg, S., Rouwkema, J., Macdonald, M., Garfein, E.S., Kohane, D.S., Darland, D.C., Marini, R., van Blitterswijk, C.A., Mulligan, R.C., D'Amore, P.A., and Langer, R. (2005). Engineering vascularized skeletal muscle tissue. Nat. Biotechnol. *23*, 879–884.

Madden, L., Juhas, M., Kraus, W.E., Truskey, G.A., and Bursac, N. (2015). Bioengineered human myobundles mimic clinical responses of skeletal muscle to drugs. eLife *4*, e04885.

Maffioletti, S.M., Sarcar, S., Henderson, A.B.H., Mannhardt, I., Pinton, L., Moyle, L.A., Steele-Stallard, H., Cappellari, O., Wells, K.E., Ferrari, G., et al. (2018). Three-Dimensional Human iPSC-Derived Artificial Skeletal Muscles Model Muscular Dystrophies and Enable Multilineage Tissue Engineering. Cell Rep. *23*, 899–908.

Mann, C.J., Perdiguero, E., Kharraz, Y., Aguilar, S., Pessina, P., Serrano, A.L., and Muñoz-Cánoves, P. (2011). Aberrant repair and fibrosis development in skeletal muscle. Skelet. Muscle *1*, 21.

Mathew, S.J., Hansen, J.M., Merrell, A.J., Murphy, M.M., Lawson, J.A., Hutcheson, D.A., Hansen, M.S., Angus-Hill, M., and Kardon, G. (2011). Connective tissue fibroblasts and Tcf4 regulate myogenesis. Development *138*, 371–384.

Motterlini, R., Kerger, H., Green, C.J., Winslow, R.M., and Intaglietta, M. (1998). Depression of endothelial and smooth muscle cell oxygen consumption by endotoxin. Am. J. Physiol. *275*, H776–H782.

Murphy, M.M., Lawson, J.A., Mathew, S.J., Hutcheson, D.A., and Kardon, G. (2011). Satellite cells, connective tissue fibroblasts and their interactions are crucial for muscle regeneration. Development *138*, 3625–3637.

Neal, D., Sakar, M.S., Ong, L.L., and Harry Asada, H. (2014). Formation of elongated fascicle-inspired 3D tissues consisting of high-density, aligned cells using sacrificial outer molding. Lab Chip *14*, 1907–1916.

Nolan, D.J., Ginsberg, M., Israely, E., Palikuqi, B., Poulos, M.G., James, D., Ding, B.S., Schachterle, W., Liu, Y., Rosenwaks, Z., et al. (2013). Molecular signatures of tissue-specific microvascular endothelial cell heterogeneity in organ maintenance and regeneration. Dev. Cell *26*, 204–219.

Novosel, E.C., Kleinhans, C., and Kluger, P.J. (2011). Vascularization is the key challenge in tissue engineering. Adv. Drug Deliv. Rev. *63*, 300–311.

Osaki, T., Sivathanu, V., and Kamm, R.D. (2018). Crosstalk between developing vasculature and optogenetically engineered skeletal muscle improves muscle contraction and angiogenesis. Biomaterials *156*, 65–76.

Perry, L., Flugelman, M.Y., and Levenberg, S. (2017). Elderly patient-derived endothelial cells for vascularization of engineered muscle. Mol. Ther. *25*, 935–948.

Potente, M., and Mäkinen, T. (2017). Vascular heterogeneity and specialization in development and disease. Nat. Rev. Mol. Cell Biol. *18*, 477–494.

Rafii, S., Butler, J.M., and Ding, B.S. (2016). Angiocrine functions of organ-specific endothelial cells. Nature *529*, 316–325.

Rall, S., and Grimm, T. (2012). Survival in Duchenne muscular dystrophy. Acta Myol. *31*, 117–120.

Ryder, S., Leadley, R.M., Armstrong, N., Westwood, M., de Kock, S., Butt, T., Jain, M., and Kleijnen, J. (2017). The burden, epidemiology, costs and treatment for Duchenne muscular dystrophy: an evidence review. Orphanet J. Rare Dis. *12*, 79.

Shandalov, Y., Egozi, D., Koffler, J., Dado-Rosenfeld, D., Ben-Shimol, D., Freiman, A., Shor, E., Kabala, A., and Levenberg, S. (2014). An engineered muscle flap for reconstruction of large soft tissue defects. Proc. Natl. Acad. Sci. USA *111*, 6010–6015.

Shimizu-Motohashi, Y., and Asakura, A. (2014). Angiogenesis as a novel therapeutic strategy for Duchenne muscular dystrophy through decreased ischemia and increased satellite cells. Front. Physiol. *5*, 50.

Stahnke, T., Kowtharapu, B.S., Stachs, O., Schmitz, K.P., Wurm, J., Wree, A., Guthoff, R.F., and Hovakimyan, M. (2017). Suppression of TGF-β pathway by pirfenidone decreases extracellular matrix deposition in ocular fibroblasts in vitro. PLoS One *12*, e0172592.

Underwood, C.J., Edgar, L.T., Hoying, J.B., and Weiss, J.A. (2014). Cell-generated traction forces and the resulting matrix deformation modulate microvascular alignment and growth during angiogenesis. Am. J. Physiol. Heart Circ. Physiol. *307*, H152–H164.

Visone, R., Gilardi, M., Marsano, A., Rasponi, M., Bersini, S., and Moretti, M. (2016). Cardiac Meets Skeletal: What's New in Microfluidic Models for Muscle Tissue Engineering. Molecules *21*, E1128.

Wynn, T.A. (2008). Cellular and molecular mechanisms of fibrosis. J. Pathol. *214*, 199–210.

Yin, H., Price, F., and Rudnicki, M.A. (2013). Satellite cells and the muscle stem cell niche. Physiol. Rev. *93*, 23–67.

Zanotti, S., Gibertini, S., Bragato, C., Mantegazza, R., Morandi, L., and Mora, M. (2011). Fibroblasts from the muscles of Duchenne muscular dystrophy patients are resistant to cell detachment apoptosis. Exp. Cell Res. *317*, 2536–2547.

Zanotti, S., Gibertini, S., Savadori, P., Mantegazza, R., and Mora, M. (2013). Duchenne muscular dystrophy fibroblast nodules: a cell-based assay for screening anti-fibrotic agents. Cell Tissue Res. *352*, 659–670.

Zanotti, S., Bragato, C., Zucchella, A., Maggi, L., Mantegazza, R., Morandi, L., and Mora, M. (2016). Anti-fibrotic effect of pirfenidone in muscle derived-fibroblasts from Duchenne muscular dystrophy patients. Life Sci. *145*, 127–136.

STAR★METHODS

KEY RESOURCES TABLE

REAGENT or RESOURCE	SOURCE	IDENTIFIER
Antibodies		
mouse monoclonal anti-α Smooth Muscle Actin	abcam	Cat#ab7817; RRID:AB_262054
mouse monoclonal anti-Fast Myosin Heavy Chain	abcam	Cat#ab51263; RRID:AB_2297993
mouse monoclonal anti-sarcomeric alpha actinin	abcam	Cat#ab9465; RRID:AB_307264
rabbit polyclonal anti-dystrophin	abcam	Cat#ab15277; RRID:AB_301813
mouse monoclonal anti-Pax7	santacruz	Cat#sc-81648; RRID:AB_2159836
rabbit polyclonal anti-collagen type I	abcam	Cat#ab34710; RRID:AB_731684
rabbit polyclonal anti-fibronectin	abcam	Cat#ab2413; RRID:AB_2262874
rabbit polyclonal anti-TSPAN7	santacruz	Cat#sc-139572; RRID:AB_10840620
mouse monoclonal anti-FGF9	santacruz	Cat#sc-373716; RRID:AB_10915599
mouse monoclonal anti-Flk1	santacruz	Cat#sc-6251; RRID:AB_628431
mouse monoclonal anti-laminin α4	thermofisher	Cat#MA5-24651; RRID:AB_2637266
mouse monoclonal anti-β tubulin I	sigma-aldrich	Cat#T7816; RRID:AB_261770
goat anti-rabbit IgG horseradish peroxidase (HRP)-conjugated polyclonal antibody	sigma-aldrich	Cat#A0545; RRID:AB_257896
goat anti-Mouse IgG HRP-conjugated polyclonal antibody	thermofisher	Cat#62-6520; RRID:AB_2533947
rabbit monoclonal anti-CD31 (biotin)	abcam	Cat#ab199734
Biological Samples		
Healthy adult muscle tissue (hip biopsy)	IRCCS Istituto Ortopedico Galeazzi	N/A
Healthy bone marrow aspirates (hip biopsy)	IRCCS Istituto Ortopedico Galeazzi	N/A
Chemicals, Peptides, and Recombinant Proteins		
gelatin from porcine skin	sigma-aldrich	Cat#G1890
6-aminocaproic acid	sigma-aldrich	Cat#A7824
human recombinant hepatocyte growth factor	peprotech	Cat#100-39
human recombinant fibroblast growth factor basic	peprotech	Cat#100-18C
human recombinant transforming growth factor β1	peprotech	Cat#100-21
Critical Commercial Assays		
Microarray	agilent	Cat#G4851C
Deposited Data		
Raw data microarray	This paper	GEO: GSE122046
Experimental Models: Cell Lines		
Immortalized human muscle myoblasts	Laboratory of Dr. Davide Gabellini (San Raffaele Hospital)	N/A
Human umbilical vein ECs	Angioproteomie	Cat#cAP-0001GFP and cAP-0001RFP
Human bone marrow-derived mesenchymal stem cells	IRCCS Istituto Ortopedico Galeazzi	N/A
Human primary ECs from muscle biopsies	IRCCS Istituto Ortopedico Galeazzi	N/A
Human fibroblasts (control and DMD)	EuroBioBank and the Telethon Network of Genetic Biobanks (GTB12001F)	N/A
Oligonucleotides		
Primers for DES, MYF5, CD31, CD36, TSPAN7, PPARG, RPL32 (see Figure S6)	This paper	N/A
Software and Algorithms		
Comsol Multiphysics 4.3b	Comsol	N/A
Fiji	http://fiji.sc/	N/A
Imaris	Bitplane	N/A

CONTACT FOR REAGENT AND RESOURCE SHARING

Further information and requests for resources and reagents should be directed to and will be fulfilled by the Lead Contact, Matteo Moretti (matteo.moretti@grupposandonato.it).

EXPERIMENTAL MODEL AND SUBJECT DETAILS

Human subjects

Human biopsies were obtained after informed consent. The study was approved by the Ethics Committee of Ospedale San Raffaele (Milan, Italy). Copy of the approval letter is available upon request. Here are detailed information of human donors:

Donor 1: 43 years old, female, Caucasian
Donor 2: 51 years old, male, Caucasian
Donor 3: 46 years old, male, Caucasian

Cell isolation and culture

Immortalized muscle cells were a kind gift of Dr. Gabellini (San Raffaele Hospital). Additional information on the isolation and characterization of muscle cells are available at https://www.umassmed.edu/wellstone as well as in a recent publication by Dr. Gabellini lab (Ferri et al., 2015). The "University of Massachusetts Medical School Senator Paul D. Wellstone Muscular Dystrophy Cooperative Research Center for FSHD" is an internationally recognized biobank providing pure populations of muscle cells from healthy and diseased donors. Muscle cells were grown in muscle growth medium (4:1 DMEM:Medium199, LifeTech, Italy) supplemented with 15% Fetal Bovine Serum (FBS, GE Healthcare Life Sciences, Italy), 2% HEPES (LifeTech), 0.03 μg/ml ZnSO4 (Sigma-Aldrich, Germany), 1.4 μg/ml vitamin B12 (Sigma-Aldrich), 0.055 μg/ml dexamethasone (Sigma-Aldrich), 1% penicillin/streptomycin/glutamine (PSG, LifeTech), 1% sodium pyruvate (LifeTech), 2.5 ng/ml hepatocyte growth factor (PeproTech, UK) and 10 ng/ml basic fibroblast growth factor (PeproTech). For myoblast fusion and differentiation, cells were switched to 4:1 DMEM:Medium199 supplemented with 2% FBS, 1% PSG and 1% sodium pyruvate.

ECs were purchased from Angioproteomie (http://www.angioproteomie.com/commerce/ccc2444-human-endothelial-cells-normal-human-endothelial-cells–human-lymphatic-endothelial-cells–stable-shrna-transfected-huvecs.htm), which is a company specialized in the isolation and characterization of ECs from different sources and tissues. The company certifies that ECs are CD31 and vascular endothelial (VE)-cadherin positive. These markers are recognized as critical indicators for EC identity. ECs were cultured in endothelial growth medium-2 (Lonza, distributed in Italy by Euroclone) up to passage 7. Primary ECs from muscle biopsies were isolated from patients undergoing hip surgery following informed consent. Cells were selected for the expression of CD31 and cultured in EGM-2 (Lonza).

Human bone-marrow derived mesenchymal stem cells (MSCs) were collected from bone-marrow aspirates of patients undergoing hip surgery following informed consent. MSCs were selected by plastic adherence and used up to passage 6 (Jeon et al., 2015). Cells were cultured using α-MEM (LifeTech) supplemented with 10% FBS, 1% penicillin/streptomycin, 1% HEPES, 5 ng/ml basic fibroblast growth factor.

Fibroblasts (control and DMD) were isolated from tissue biopsies based on previously established protocols (Zanotti et al., 2011, 2013). Briefly, fibroblasts were isolated from connective tissue chunks of muscle biopsies. Connective tissue was minced in small pieces and plated on standard plastic dishes. Outgrowth cells were collected and expanded up to passage 4. Muscle fibroblasts were cultured using DMEM supplemented with 10% FBS, 1% penicillin/streptomycin and 5 ng/ml basic fibroblast growth factor. The same medium was used for culturing DMD fibroblasts. Cytokine treated fibroblasts were cultured in presence of 10 ng/ml TGF-β1 (Peprotech).

METHOD DETAILS

Construct frame fabrication

Arch-shaped 3D structures were fabricated by 3D printing of Clear Resin Formlabs (Formlabs Inc., USA). The gap size within the arch-shaped structure was 2x2x4 mm^3 (2x2 mm^2 is the cross-sectional area). Cells were embedded within this gap size. This 2x2x4 mm^3 gap was encased in a structure whose dimension was 5x4x4 mm^3. The diameter of the side through-holes was 600 μm. The structures were irreversibly glued to a glass coverslip and sterilized with iso-propanol before use.

Computational simulations

The oxygen consumption-diffusion was modeled with Comsol Multiphysics. The model considered the presence of a 3D fibrin matrix embedding ECs and 3 fibers of muscle cells. Cell constructs were modeled with 1,000,000 tetrahedral elements. Atmospheric oxygen level was assumed at the 2 lateral openings of the 3D arch-shaped structure and at the side through-holes for muscle cell injection. All other boundaries were assigned as "no flux" boundary conditions in order to reproduce the presence of the oxygen impermeable arch-shaped structure. The oxygen diffusion coefficient was assumed equal to 2 × 10-9 m^2/s (Colom et al., 2014).

The oxygen consumption was assumed to be 5.51 × 10-5 mol/(m^3 × s) for ECs (Abaci et al., 2011) and 3.23x10-4 mol/(m^3 × s) for muscle cells (Motterlini et al., 1998). A Michaelis-Menten kinetics was assumed for ECs considering a Michaelis constant of 5.5x10-4 mol/m^3 (Abaci et al., 2011).

3D Construct preparation

Preparation of muscle fibers was performed adapting previously described protocols (Neal et al., 2014). Three steel rods (600 μm diameter) were first inserted into the three side holes of the 3D arch-shaped structures. A warm solution of porcine skin gelatin (50 mg/ml, Sigma-Aldrich) in muscle growth medium supplemented with 2.5 mg/ml 6-aminocaproic acid (Sigma-Aldrich) was pipetted in the central frame gap and cooled at 4°C for 15'. The steel rods were pulled out of the frame forming three cylindrical cavities in the cooled gelatin. Highly concentrated human myoblasts (20M cells/ml) were 1:1 mixed with a fibrin gel solution (5 mg/ml) and immediately injected in the cavities. The gel was allowed to polymerize for 15' at room temperature. The constructs were then immersed in 1 mL muscle differentiation medium for 5 days to dissolve gelatin and induce myoblast differentiation. A second fibrin gel (5 mg/ml) was then prepared to surround the differentiated muscle fibers and 1:1 mixed with different cell suspensions: 2.5M cells/ml ECs alone; 2.5M cells/ml ECs: 0.25M cells/ml MSCs; 2.5M cells/ml ECs: 0.25M cells/ml muscle-derived fibroblasts. The constructs were dried by pipetting medium out of the central gap and the fibrin gel solution was subsequently injected. The gel was allowed to polymerize for 15' at room temperature in humidity chambers. The constructs were then immersed in 1 mL EGM-2 and cultured for additional 3 or 6 days.

Regarding 3D constructs for muscle monocultures, cells were embedded in the matrix at the same density used for the development of the 3D muscle fibers (10 Mcells/ml). The constructs were then kept in culture for the same amount of time of 3D muscle fibers.

Immunofluorescence

Constructs were fixed with 2.5% paraformaldehyde for 30 min. Permeabilization and blocking steps were performed with Triton X-100 (0.1%) and Bovine Serum Albumin (5%). Cells were then probed with the following primary antibodies (overnight at 4°C): anti-α Smooth Muscle Actin (1:60, mouse anti-human, Abcam, distributed in Italy by Prodotti Gianni) to highlight differentiation of MSCs into mural cells; anti-Fast Myosin Heavy Chain (1:100, mouse anti-human, Abcam), anti-sarcomeric alpha actinin (1:100, mouse anti-human, Abcam) and anti-dystrophin (1:100, rabbit anti-human, Abcam) to highlight muscle cells differentiation; anti-Pax7 (1:100, mouse anti-human, Santa Cruz, distributed in Italy by DBA) for satellite cells; anti-collagen type I (1:250, rabbit anti-human, Abcam) and anti-fibronectin (1:200, rabbit anti-human, Abcam) for ECM protein deposition; anti-TSPAN7 (1:25, rabbit anti-human, Santacruz) for EC differentiation. Samples were washed with Phosphate Buffered Saline (PBS) and overnight incubated with secondary antibodies at 4°C (Alexa Fluor 488 or Alexa Fluor 568 or Alexa Fluor 647). Vybrant cell labeling (DiD, LifeTech) was employed to track muscle-derived fibroblasts. Nuclear staining was performed with DAPI whereas actin fibers staining was performed with Phalloidin.

Image acquisition and analysis

High-resolution images of the constructs were acquired with a two-photon confocal microscope (Nikon A1R MP+ with Coherent UltraII). Images for vascular network quantifications were acquired with confocal microscope (Leica TCS SP2). Fiji software (http://fiji.sc/) and Imaris software (Bitplane) were used for image analysis. Imaris software was employed to capture qualitative images of the vascular network skeleton using the FilamentTracer plugin.

For quantification of fibroblast recruitment, we employed Fiji to design 100 × 100 μm^2 regions along multiple fibers collected in different experiments. We quantified the recruitment as the area fraction covered by fibroblasts (white color in Figure 5) in each ROI for each different condition. Data were obtained from 3 independent experiments.

Regarding matrix protein deposition in 2D and 3D, we employed Fiji to design 200 × 200 μm^2 regions and we quantified the fluorescence intensity of each specific antibody in each ROI for each condition. Data were obtained from 3 independent experiments.

Cell sorting

Hydrogels were digested using 50 U/ml nattokinase (JBSL-USA) under stirring for 30 min at 37°C. Next, single cell populations were sorted. Briefly, cells were incubated with biotinylated anti-CD31 (Abcam) for 10' at 4°C under stirring. Streptavidin coupled dynabeads (LifeTech) were then added and incubated for 20 min at 4°C under stirring. Following interaction with the magnet, anti-CD31 labeled ECs were collected while muscle cells were obtained from the supernatant. Each cell population was then used for gene expression analyses.

qRT-PCR and Microarray analyses

Total RNA of each cell population (cells isolated from 3D vascularized muscle models, 3D ECs monocultures, primary ECs from human muscle biopsies) was extracted by using the PureLink RNA Mini Kit (Ambion, Italy). cDNA was obtained using the iScript cDNA Synthesis Kit (Bio-Rad, Italy). Gene expression of selected markers was analyzed by qRT-PCR. The following primers were employed for ECs: CD36, CD31, TSPAN7 and PPARG. Muscle cells were analyzed using the following probes: MYF5 and Desmin. Details are reported in Figure S6. Three experimental replicates were analyzed for each marker. ECs were analyzed after 3 days co-culture with muscle cells (or 3 days monoculture for control samples). The gene expression was normalized to the housekeeping

gene ribosomal protein L32 (RPL32) and to the experimental control (3D ECs monocultures or muscle cells monocultures) using the 2-ΔΔCt method.

Regarding Microarray analyses, total RNA of ECs was extracted following the same procedure described above. Libraries were then prepared according to the manufacturer protocol (Agilent). The comparison involved 2 independent biological replicates of ECs after co-culture with muscle cells and 3 different populations of primary muscle-derived ECs from 3 different donors.

Western Blot

ECs were cultured or co-cultured for 3 days and then sorted. The cells were lysed in NP40 buffer, supplemented with a protease inhibitor cocktail and 1 mM phenylmethylsulfonyl fluoride (PMSF; Sigma-Aldrich, Saint Louis, MO, USA) for 30 min on ice, then centrifuged at 13,000 r/min for 10 min at 4°C, and the supernatant was stored at −20°C until assayed. Protein content was determined with the Pierce® BCA protein assay (Thermofisher, Waltham, MA, USA). Proteins (15 μg) were loaded on 8% sodium dodecyl sulfate (SDS)-polyacrylamide gels and then then electroblotted onto Hybond-P polyvinylidene difluoride transfer membranes (BioRad Laboratories, CA, USA). After blocking (5% non-fat dry milk in PBS, 30 min, room temperature), the membranes were incubated overnight at 4°C with 1:10 rabbit polyclonal anti-human TSPAN7 (sc-139572, Santa Cruz Biotechnology Dallas, TX, USA), 1:100 mouse monoclonal anti-human FGF-9 (sc-373716, Santa Cruz Biotechnology), 1:200 mouse monoclonal anti-human Flk-1 (sc-6251, Santa Cruz), 1:1000 mouse monoclonal anti-human Laminin α-4 (MA5-24651, Thermofisher). β-Tubulin I was used as housekeeping by means of 1:20000 mouse monoclonal anti-human β-Tubulin I (T7816, Sigma-Aldrich), all of them in 5% non-fat dry milk in PBS. After washing with tween-supplemented tris-buffered saline (TBS-T) 0.3% for 30 min, the membranes were incubated for 1 h at room temperature with a goat anti-rabbit IgG horseradish peroxidase (HRP)-conjugated polyclonal antibody (1:5000; A0545; Sigma-Aldrich), or goat anti-Mouse IgG HRP-conjugated polyclonal antibody (1:5000, 62-6520 Thermofisher), and developed with a chemiluminescence enhancement kit (Clarity Max Western ECL Substrate, BioRad, Hercules, CA, USA). Band densities were quantified from digital acquisition by a Chemidoc Imaging System (Biorad) using NIH ImageJ software.

QUANTIFICATION AND STATISTICAL ANALYSIS

Unpaired Student's t test and one-way analysis of variance (ANOVA) were performed using Prism Graph Pad. Data were first analyzed for normality and then compared with parametric statistics. Differences were considered significant with $p < 0.05$ (*), $p < 0.01$ (**) and $p < 0.001$ (***). Results are presented as mean ± standard error of the mean (SEM). Details are reported in each figure.

DATA AND SOFTWARE AVAILABILITY

The accession number for the Microarray data reported in this paper is GEO: GSE122046.